Journal of Oceanography, Vol. 65, pp. 721 to 736, 2009

A Numerical Study of the Seasonal Circulation in the Seto Inland Sea, Japan

PIL-HUN CHANG[1]*, XINYU GUO[2] and HIDETAKA TAKEOKA[2]

[1]*National Institute of Meteorological Research, Kisangcheng-gil, Dongjak-gu, Seoul 156-720, Korea*
[2]*Center for Marine Environmental Studies, Ehime University, Bunkyo-cho, Matsuyama 790-8577, Japan*

(Received 3 February 2009; in revised form 17 March 2009; accepted 12 June 2009)

The seasonal variation of water circulation in the Seto Inland Sea is investigated using a high resolution, three-dimensional numerical ocean model. The model results are assessed by comparison with long-term mean surface current and hydrographic data. The simulated model results are consistent with observations, showing a distinct summer and winter circulation patterns. In summer the sea water is highly stratified in basin regions, while it is well mixed near the straits due to strong tidal mixing there. During this period, a cold dome is formed in several basins, setting up stable cyclonic eddies. The cyclonic circulation associated with the cold dome develops from May and disappears in autumn when the surface cooling starts. The experiment without freshwater input shows that a basin-scale estuarine circulation coexists with cyclonic eddy in summer. The former becomes dominant in autumn circulation after the cold dome disappears. In winter the water is vertically well mixed, and the winter winds play a significant role in the circulation. The northwesterly winds induce upwind (downwind) currents over the deep (shallow) water, forming a "double-gyre pattern" in the Suo-Nada, two cyclonic eddies in Hiuchi-Nada, and anticyclonic circulation in Harima-Nada in vertically averaged current fields.

Keywords:
· Numerical simulation,
· general circulation,
· seasonal variation,
· cold dome,
· cyclonic eddy,
· wind-induced circulation,
· Seto Inland Sea.

1. Introduction

The Seto Inland Sea (SIS), located in western Japan, is a semi-enclosed, elongated coastal region (Fig. 1). It has a unique geographical feature, consisting of several basins (called "*Nada*" in Japanese), such as Suo-Nada, Iyo-Nada, Hiuch-Nada and Harima-Nada, which are connected with each other through narrow straits. The SIS opens to the Pacific Ocean via the Bungo and Kii Channels, through which a tidal wave with similar phase propagates into the Inland Sea to converge near the Bisan Strait. Due to these geographical features, tidal mixing is strong near the straits and relatively weak in Nada (refer to figure 4 of Yanagi and Okada, 1993). Such regional difference in tidal mixing in the SIS determines the spatial distribution of density stratification in summer (e.g., Takeoka, 1985).

The character of the water in the SIS is strongly seasonal. The great freshwater runoff from rivers (see Fig. 2 for the location of major rivers) and rainfall produce low-salinity water during summer. For example, a water mass with salinity of about 31 psu distributes widely in Harima-Nada in summer. In combination with the freshwater input, the heat flux from spring to summer gives rise to summer stratification in the basins where tidal mixing is relatively weak. It also should be mentioned that a dome-shaped bottom cold water mass (hereinafter, cold dome) is formed in several Nadas; for instance, the cold dome with anoxic water and/or cyclonic flow has been studied in Hiuchi-Nada (e.g., Ochi and Takeoka, 1986; Guo *et al*., 2004; Kasai *et al*., 2007); residual flow related to cold dome was investigated in Iyo-Nada (Guo *et al*., 2006). In addition, hydrographic observation along the SIS during summer has revealed a cold dome in Iyo- and Harima-Nada (Kobayashi *et al*., 2006), similar to Fig. 6(b) (shown later).

The abovementioned circulation features related to the cold dome have also been studied in other seas where stratified water is surrounded by vertically homogeneous

* Corresponding author. E-mail: phchang@korea.kr

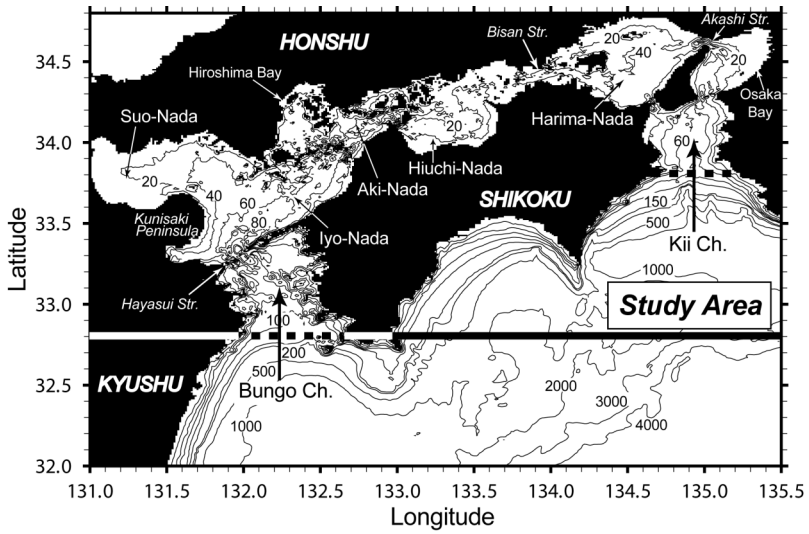

Fig. 1. Model domain and bathymetry. Thick solid line indicates southern boundary of present prognostic model. Results of a diagnostic model that covers the whole domain are imposed along the open boundaries, i.e., dotted lines at the entrance to Bungo and Kii Channels. Water depths are in meters.

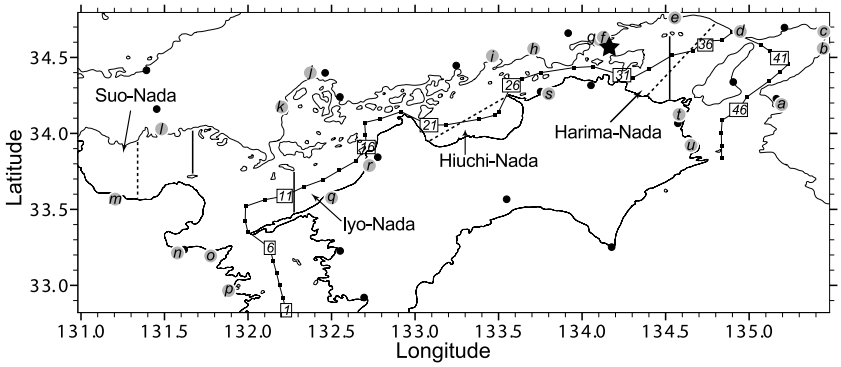

Fig. 2. Locations of samples and sections. Small squares indicate samples of hydrographic data for model validation (see Figs. 6 and 7), and solid dots are meteorological stations for calculation of short-wave radiation. The SST observation station is represented by a solid star in northern Harima-Nada. Circles with letters along the coast are the location of river inflow (see Table 1 for annual mean discharge). Sections across eddies in summer and winter circulations are denoted by solid and dotted lines, respectively. See Figs. 9(b) and 13 for eddies calculated in summer and winter, respectively.

water. For example, through extensive field observations, Hill (1994) revealed the presence of a cold dome and its relationship with cyclonic eddy in the Irish Sea in summer. The observed cyclonic circulation was subsequently studied with a two-layer (Hill, 1996) and three-dimensional models (e.g., Xing and Davis, 2001; Horsburgh and Hill, 2003).

On account of surface cooling the water is homogeneous through the whole water column over the SIS in winter. During this period, a northwesterly wind prevails over the sea surface (refer to Fig. 3(d)), which is expected to play an important role in the water circulation. For example, Fujiwara and Higo (1986) suggested that the winter wind enhances eastward volume transport in the SIS. Despite its importance, its role in the winter circulation in the SIS has not been well understood hitherto, partly due to the difficulties measuring currents and partly due to a comparative lack of modeling effort.

As mentioned above, it is anticipated that seasonally varying surface momentum, heat and salt fluxes, and river discharge possibly cause a unique seasonal circulation in the SIS, competing with regional difference in tidal mixing. However, little effort has been expended so far in understanding the seasonal variation of general circu-

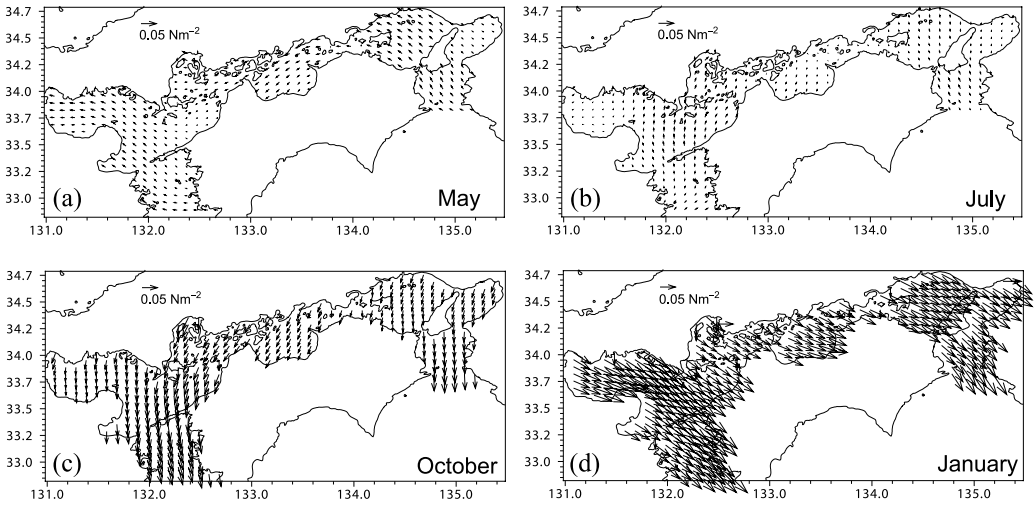

Fig. 3. Monthly mean wind stress fields in (a) April, (b) July, (c) October and (d) January.

lation in the SIS, in particular from the viewpoint of the entire SIS. Since the tidal effect is important in the SIS, many numerical simulations have been performed to investigate the tides and tide-induced residual flow (e.g., Oonishi, 1977), tidal exchange near the narrow strait (Awaji *et al*., 1980; Imasato *et al*., 1980), and the effect of tidal stirring on density stratification (Takeoka, 1985; Kobayashi *et al*., 2006). In addition, density-induced circulation in the SIS has been examined using a diagnostic numerical model (Murakami *et al*., 1978, 1985; Yanagi and Igawa, 1992; Guo *et al*., 2004). As Takeoka (2002) pointed out, most numerical studies of the SIS circulation have focused on the individual processes, such as tides, tide-induced residual flow, density-driven currents, and water exchange. Furthermore, most of these studies were limited to a basin scale, or else they dealt with the entire SIS as one-dimensional channel system. Thus, there is still no comprehensive numerical study of seasonal circulation in the SIS.

In the present study a high-resolution, three-dimensional numerical model is applied to the SIS to examine the seasonal variation of water circulation. Besides the tidal forcing, the model is forced by monthly surface fluxes, river run-off and oceanic lateral fluxes via the Bungo and Kii Channels. Here we mainly examine the seasonal variability of general circulation and the forcings determining seasonality.

2. Model Description

The numerical ocean model adopted in this study is based on the Princeton Ocean Model (POM), described in detail by Blumberg and Mellor (1987). The POM is a three-dimensional, primitive-equation, sigma-coordinate model. It incorporates thermodynamics and the second momentum turbulent closure scheme of Mellor and Yamada (1982) to calculate vertical mixing coefficients. In addition, horizontal mixing coefficients are parameterized using a Smagorinsky (1963) formulation.

The POM is applied to the SIS for prognostic modeling studies. Figure 1 shows the model domain and bottom topography. The model grid has a resolution of about 1 km in the horizontal (1/120 degree in meridianal direction and 1/80 degree in zonal direction), and 21 sigma levels in the vertical. Bottom topography is obtained from the Japan Oceanographic Data Center (JODC) dataset with 1 km resolution. The bathymetry data in some regions, however, are somewhat incorrect, so they have been modified by depth data read from a nautical map. The minimum depth is set to 5.0 m.

The monthly surface fluxes used to drive the model include surface momentum, heat and water fluxes. The wind forcing is based on a recent 3-year (2003–2005) results of wind velocity from Grid Point Value of Meso-Scale Model (GPV-MSM) provided by Japan Meteorological Agency (JMA). The monthly wind stress is computed from the wind velocity of GPV-MSM with 6 hour and 10 km resolutions at 10 meters height, adopting the drag coefficient of Large and Pond (1981). Figure 3 shows seasonal variation of wind stress in the SIS. In general, the spring wind is weak and its direction is region-dependent. In July, southeasterly and southerly winds are dominant but the stress is still relatively small. Thereafter, northerly winds commence in October. In January, intense northwesterly wind stress covers the whole SIS.

The net surface heat flux, Q, excluding the shortwave radiation, is calculated by:

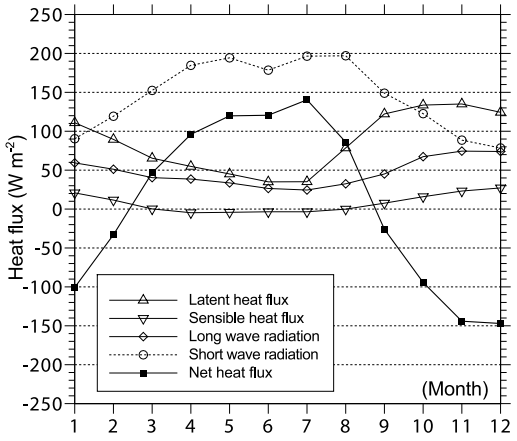

Fig. 4. Seasonal variations of long-wave radiation, sensible and latent heat fluxes at the station in Harima-Nada, spatially averaged short-wave radiation over whole model domain and the sum of four components of heat flux, i.e., net heat flux.

$$Q = Q_O + \gamma_T \left(T - T_{clim.}\right), \tag{1}$$

where Q_O is the surface heat flux. The monthly mean Q_O of is computed by adopting bulk formulae described by Hirose *et al*. (1999), utilizing daily sea surface temperature (SST) observed at a coastal station in Harima-Nada by the Fisheries Experiment Station Okayama Prefecture and the atmospheric data from the meteorological station in Okayama during 23 years (1974–1996). The locations of the coastal station for SST and the meteorological station are given in Fig. 2. The calculated Q_O is applied uniformly throughout the model domain and is modified to Q by the second term in (1), in which T is the calculated SST, and $T_{clim.}$ is the monthly mean SST based on the Marine Information Research Center (MIRC) dataset covering 30 years, and γ_T is chosen as –40.0 W m^{-2}degree^{-1}. The short-wave radiation Q_s is calculated by the formula of Kim and Kimura (1995), using daily fractional cloud cover observed at 19 meteorological stations (see the location in Fig. 2) around the SIS during 1974–1996. Figure 4 shows the seasonal variation of spatially averaged Q_O (i.e., long-wave radiation, sensible and latent fluxes) and short-wave radiation Q_s.

Surface salinity flux, W_s is calculated as follows:

$$W_s = (P - E)S + \gamma_S \left(S - S_{clim.}\right). \tag{2}$$

For the term γ_S we adopted the weak value of –10.0/365 m day^{-1}. P and E are precipitation and evaporation given by Tawara (1986). S is calculated surface salinity, $S_{clim.}$ and is climatological monthly surface salinity from MIRC dataset.

Table 1. Annual mean river discharges of 21 major rivers in the Seto Inland Sea, based on the 8-year (1993–2000) dataset of Ministry of Land, Infrastructure and Transport (MLIT). The location of river mouths is shown in Fig. 2.

No.	River	Discharge (m^{3}s^{-1})
a	Kino	48.63
b	Yamato	26.27
c	Yodo	242.42
d	Kako	43.56
e	Ibo	27.33
f	Yoshii	63.25
g	Asahi	55.43
h	Takahashi	64.61
i	Ashida	11.50
j	Oota	76.74
k	Oze	12.84
l	Saba	17.67
m	Yamakuni	21.03
n	Oita	27.25
o	Oono	62.28
p	Bansho	14.26
q	Hiji	37.84
r	Sigenobu	8.93
s	Doki	1.97
t	Yoshino	37.70
u	Naka	61.28

The present prognostic model employs the results of a *robust* diagnostic model, which was previously used for Hiuchi-Nada (Guo *et al*., 2004), as boundary conditions at the open boundaries (i.e., Bungo and Kii Channels). The grid size and bathymetry of diagnostic model are the same as in the present model, while the south boundary of the diagnostic model extends to 32°N (see Fig. 1), including the Kuroshio region. The initial temperature and salinity fields used in diagnostic model are produced by merging the MIRC dataset in the SIS region and the model results of Guo *et al*. (2003) in the Kuroshio region. Twelve cases of diagnostic calculations, corresponding to 12 months, were performed by adopting monthly density and wind fields mentioned above. The de-tided velocity, temperature, salinity, and surface elevation obtained from the diagnostic model are then specified along the open boundary of the prognostic model (see thick dotted line in Fig. 1). Along the open boundary, tidal forcing due to four major tidal constituents M_2, S_2, O_1 and K_1, provided by Matsumoto *et al*. (2000), are also linearly superimposed on the sub-tidal fields from the diagnostic model.

In the prognostic model the normal velocity along the open boundary, U_n, is computed according to the Flather (1976) radiation condition:

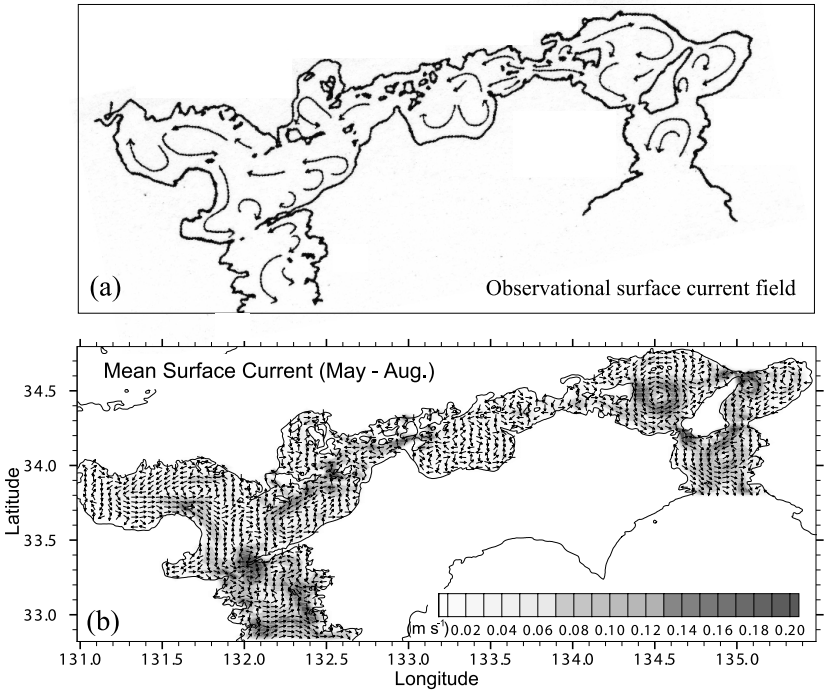

Fig. 5. Surface residual current distributions. (a) Schematic map of annual mean residual current based on the observations (Yanagi and Higuchi, 1979) and (b) simulated current distribution averaged from May to August. See text for explanation of the reason why we use current field averaged from May to August.

$$U_n = U_{Diag.} + U_T + \sqrt{g/H}\left(\eta - \eta_T - \eta_{Diag.}\right), \qquad (3)$$

where $U_{Diag.}$ and $\eta_{Diag.}$ represent de-tided normal velocity and surface elevation from the diagnostic model, respectively. U_T and η_T denote the tidal flow and the tidal elevation computed using the harmonic constants of four major tidal components, provided by Matsumoto *et al.* (2000). η denotes predicted sea elevation in the model, and H water depth along the open boundary.

The present model includes major 21 rivers, of which the locations are shown in Fig. 2. The monthly river discharges averaged over 8 years (1993–2000), reported by Ministry of Land, Infrastructure and Transport (MLIT), were used in the calculation. The annual variation of all river discharges shows that the discharge reaches its maximum (2.08×10^3 m^3s^{-1}) in July and minimum (0.49×10^3 m^3s^{-1}) in December. In general, large rivers, in terms of volume discharge, are located along the northern coasts of SIS, as can be understood from the annual mean discharges of each river (Table 1).

The initial temperature and salinity fields in January are from the MIRC dataset, and then the model was run for two years. All the monthly forcings on the surface and lateral boundaries were interpolated linearly in time at each time step. Here, results in the second year are used to describe the circulation in the SIS.

3. Comparison between Model Simulations and Observations

3.1 Validation of surface current fields

To assess the model's performance, in this section we compare surface currents fields and hydrography between observations and simulated results. As briefly mentioned in Section 1, the observed current data covering the entire SIS are not sufficient to describe the seasonal water circulation. Yanagi and Higuchi (1979) collected observed surface current data and depicted annual-mean residual flow for the entire SIS. However, a large number of those collected data were observed in the period from May to August. Thus, although part of their data was obtained in other seasons, their annual mean flow basically represents the current distribution in late spring and summer.

Here we first compare the schematic map of surface current (Fig. 5(a)) given by Yanagi and Higuchi (1979), and the simulated result averaged from May to August (Fig. 5(b)). In the observation and model results, large cyclonic and anticyclonic eddies are developed near the entrance and inner part of Suo-Nada, respectively. These two eddies were also suggested from the movement of drift bottles observed during the spring season (Kamizono *et al.*, 1991) and a diagnostic model forced by monthly hydrographic data in warm seasons (Balotro *et al.*, 2002).

Associated with the well-developed large cyclonic eddy in Suo-Nada, the southward flow hugging Kunisaki Peninsula reaches Hayasui Strait in both the observed and model results. In our model, the southward flow has a magnitude of 0.1–0.2 m s^{-1} during the warming season and is strengthened in autumn (shown later in Fig. 9(c)). Based on the long-term mean current fields observed during June through October, Tawara (1986) also pointed out that a strong southward current of 0.2–0.3 m s^{-1} was seen along the Kunisaki Peninsula. He also mentioned that the southward current become weak in winter, as shown in our model (refer to Fig. 9(d)). The model seems to illustrate the southward current flowing to the western Bungo Channel via the Hayasui Strait. In the eastern part of Bungo Channel, however, the current direction in the model turns out to be northward, while that in the observed direction is southward.

Observation shows an apparent southwestward current in the northern Iyo-Nada. A strong southwestward current (over 0.15 m s^{-1}) also appears in the model, and a cyclonic eddy coexists with this outward current, as recent field observations have reported (Guo *et al*., 2006). The observed result indicates that the southward current from the Bisan Strait is directed to the center of Hiuchi-Nada, where it bifurcates into the eastern and western sides. Analogous patterns are shown in the model, but the velocity seems to be weak.

The model also well reproduces the observed circulation features in the Harima-Nada, showing two eddies. In Osaka Bay, the southward current along the eastern coast and anticyclonic flow near the Akashi Strait are found in both the observed and model results. Fujiwara *et al*. (1989) described the residual current system in Osaka Bay, and the present model results coincide well with their conclusions. Moreover, a cyclonic eddy is clearly seen in Kii Channel in both the observed and model results. In the model, the outflow with a magnitude of 0.1–0.25 m s^{-1} from Osaka Bay to Kii Channel is directed to the western part of the channel (also, refer to Fig. 9(b)). Similar surface current fields have been shown in previous observations. On the basis of ADCP observation in summer 1996, Fujiwara *et al*. (1997) demonstrated that the outflow over 0.1 m s^{-1} from Osaka Bay turns to the western Kii Channel due to the cyclonic eddy existing around 34°N. Tawara (1986) also showed that a southward surface current of about 0.2 m s^{-1} existed along the western Kii Channel.

Simulated currents in some regions, such as the northern coast of Harima-Nada and Bungo Channel, however, differ from the observed patterns. One possible cause might arise from the different observation periods. For instance, the coastal current in northern Harima-Nada exhibits strong seasonality in our model; it is westward in summer and eastward in winter (shown later in Fig. 9).

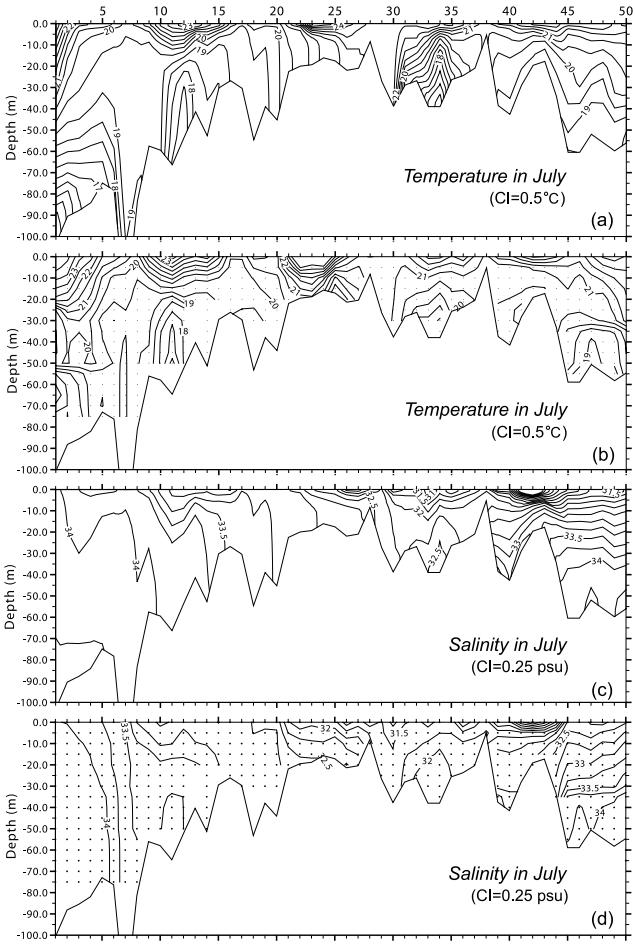

Fig. 6. Vertical distributions of calculated temperature and salinity, (a) and (c), along a section across the whole Seto Inland Sea in July (see Fig. 2 for location of stations). Also shown are those for the observation, (b) and (d). The dots in (b) and (d) denote data depths.

This means that there is a limitation to comparing all the observed current patterns with the model results. Nevertheless, the overall features of modeled surface currents are qualitatively quite consistent with the observations.

3.2 Summer and winter hydrography

In addition to the surface current fields, here we compare the vertical distributions of temperature and salinity along the SIS, as between observation and model (Figs. 6 and 7; sample locations adopted are depicted in Fig. 2). Observed results are based on the 30-year MIRC dataset. Figure 6 shows the temperature and salinity sections of the model and observation in July. In general, both model and observed results exhibit quite well the mixed water around the straits and the well stratified water in the Nadas. In temperature sections (Figs. 6(a) and (b)), sur-

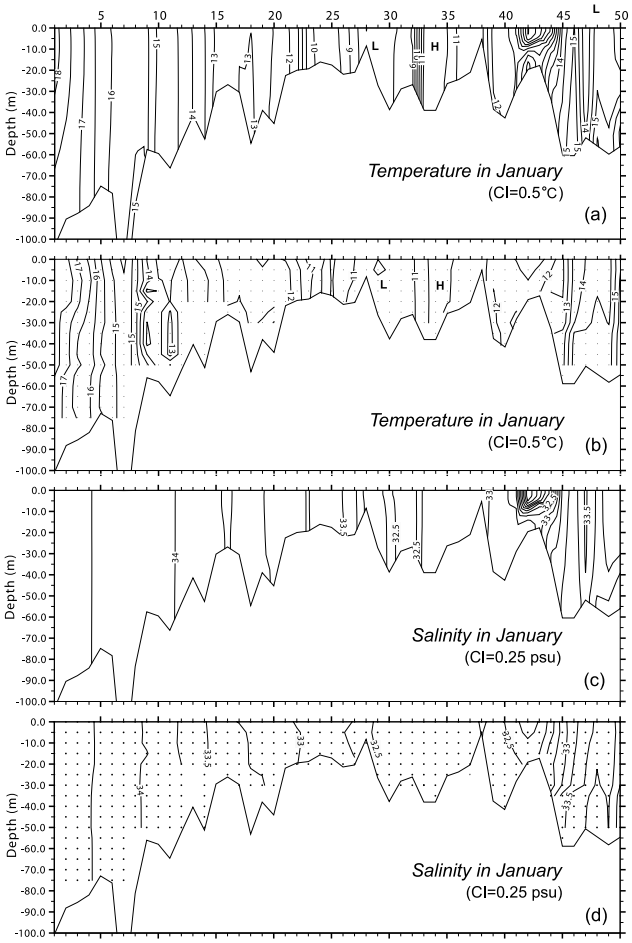

Fig. 7. As Fig. 6, but for January.

face warm pools and bottom cold water are formed in the Nadas. Similar to the observations, a cold dome is well established in Iyo-Nada, Harima-Nada and Kii Channel in the model (Fig. 6(a)). However, the calculated temperature at the Bisan Strait (i.e., areas of 27–30 in Fig. 2) is higher than that the observed value, and the bottom temperature in Harima-Nada is lower than that observed by about 2.5°C (area 34). Consequently, a strong bottom front in Harima-Nada is shown in our model.

Since the present model does not consider all river discharges in the SIS, the spatially-averaged salinity in the entire SIS is slightly higher in the model than the observed value (Figs. 6(c) and (d)). Nevertheless, the simulated results quite well represents the observed salinity pattern. The less saline water covers the entire SIS during summer, except for Bungo Channel. In particular, strong salinity stratification is detected near Osaka Bay, the location of the largest river in terms of freshwater volume discharge (see areas 40–45). Moreover, the vertical salinity variation is greater in the Kii Channel than in the Bungo Channel. Toward Bungo and Kii Channels, less saline water flows outward in the surface layer.

Figure 7 shows vertical distributions of temperature and salinity in winter. The model and observed results show the well-mixed water through the water column in the entire SIS. In general, warm water distributes in Bungo and Kii Channels, and water temperature becomes lower toward the inside SIS (Figs. 7(a) and (b)). The lowest temperature is detected in Bisan Strait in both model and observed value, although the model result is about 2.0°C higher than the observation (see samples near 30). Simulated temperature in Harima-Nada and Osaka Bay is similar to the observed value, showing about 11.0°C and 12°C, respectively (see samples near 34 and 40).

Similar to the summer, the modeled salinity in winter is higher about 0.25–0.5 psu than the observed value, probably due to the underestimation of river discharges into the model domain. However, the overall feature is similar to the observed pattern; high salinity water over 34 psu is found in Bungo Channel, and relatively low salinity water appears in the eastern part of SIS (Figs. 7(c) and (d)). In addition, cold, less saline water exists in the opening of Osaka Bay (areas of 40–45), forming a front structure against the relatively warm, saline water in Kii Channel.

4. Model Results: Circulation Inferred from the Model

In this section we examine water circulation in the SIS inferred from the model results. Since our major concern is to investigate the seasonal variation of circulation, we subtract tide-induced residual current from tidally averaged mean current. To do this, we begin with tide-induced residual current in the next subsection. In addition, we describe other experiments without wind stress (i.e., the without-wind case) in Subsection 4.4 to elucidate its role in the winter circulation.

4.1 Tide-induced residual current

The tide-induced residual current is obtained by running the 3-D ocean model (i.e., POM) driven only by the tidal forcing. The bathymetry and harmonic constants mentioned in Section 2 are given, and are also the same conditions as those used by Guo (2005). The homogeneous density field is applied in the calculation. The simulated tides and tidal flow are almost the same as their results (Guo, 2005), which present model validation and detailed results on tides and tidal flows. Figure 8 displays computed tide-induced residual currents. The simulated tide-induced residual current exhibits similar features to those shown in previous numerical studies; for example, anticyclonic eddies in the vicinity of Akashi Strait (Oonishi, 1979; Fujiwara *et al.*, 1994) and a cyclonic residual current near the western Hiuchi Nada (Guo *et al.*, 2004). On the whole, the tide-induced residual current is

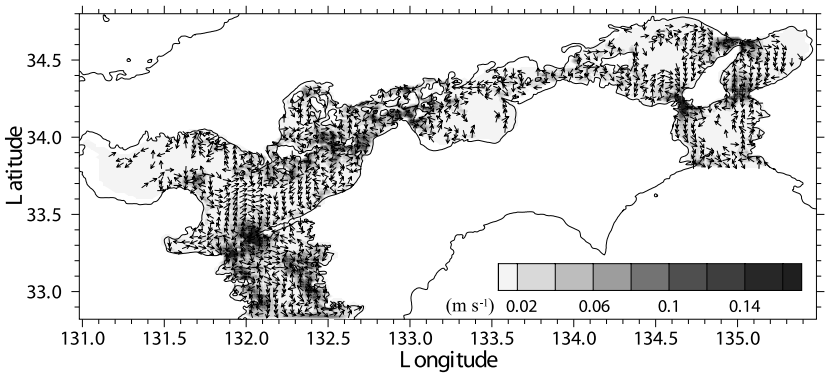

Fig. 8. Tide-induced surface residual current at 10 m depth. Tones indicate magnitude of velocity in m s^{-1}. Currents weaker than 0.005 m s^{-1} are omitted to avoid overcrowding.

strong near the straits (>0.06 m s^{-1}), while it is relatively weak in the Nadas and Kii Channel.

4.2 Seasonal variation of current fields

In this section we investigate the seasonal variation of surface and bottom current fields based on the model results. In order to present seasonally varying flow fields (i.e., density- and wind-driven flows), the calculated Eulerian tide-induced residual currents described in the above subsection are removed from tidally averaged current fields. Hereinafter, we describe the modeled monthly current fields in April, July, October, and January, defined as representative months in spring, summer, autumn, and winter, respectively (Figs. 9 and 10). In April, the northward warm current from the open sea is clearly seen in the surface layer of Bungo Channel, and the current extends to the western Iyo-Nada forming a large anticyclonic circulation at the north to Hayasui Strait (Fig. 9(a)). Furthermore, the distinct cyclonic circulation is shown in Kii-Channel. In general, the circulation inside SIS in spring is weak, compared to the circulation in summer.

Current distribution in July is similar to Fig. 5(b), showing several cyclonic eddies in the Nadas (Fig. 9(b)). In our model those eddies are formed from May when the thermal stratification begins, to become fully developed in July. In addition to these eddies, two basin scale outflow systems toward Bungo and Kii Channels are shown in the surface layer, as suggested by Murakami *et al.* (1985): an outward flow from Suo- and Aki-Nada via Bungo Channel in the western SIS, and a coastal current at the southern Harima-Nada and the flow connecting from Osaka Bay to western Kii Channel in the eastern SIS. Since wind stress is not strong (Fig. 3(b)), it is natural to anticipate that the surface current in July could be density-driven. The cyclonic eddies related to density structure will be described in the next subsection.

Eddies that were dominant in Suo-, Iyo- and Harima-Nada during summer are no longer discernable in October (Fig. 9(c)). It is, however, interesting that the strong outward flows in summer are still dominant in the surface layer. The southward flow hugging Kunisaki Peninsula reaches 0.17 m s^{-1}, which is its maximum throughout the year. The current from Aki-Nada now reveals a northwestward excursion to the entrance of Suo-Nada, where it merges with the southward flow offshore Kunisaki Peninsula. In Contrast to the summer case, an anticyclonic circulation now forms in Kii Channel, and the strong outward flow of about 0.1–0.2 m s^{-1} from Osaka Bay merges with it and flows out via the eastern part of the channel.

In January, when the water is destratified and the northwesterly wind stress is strong, the current becomes weak, except for regions near the open sea (Fig. 9(d)). The southward flow and a strong anticyclonic circulation are dominant on the surface layer in Bungo Channel and the western Iyo-Nada, respectively. In addition, a southward coastal current appears along the eastern side of Bungo and Kii Channels. Although the flow velocity is weak, it is likely that parts of the anticyclonic flow in the western Iyo-Nada penetrate into the Suo-Nada. In Harima-Nada, an eddy-like flow with a magnitude of about 0.03–0.05 m s^{-1} is found in the surface layer.

Figure 10 shows the current distribution near the bottom layer (i.e., 20th layer in the model) in the corresponding month of Fig. 9. Compared to the surface currents, the flow in the bottom layer is relatively weak and unorganized. Moreover, it is generally directed to the inner sea during summer and autumn when the less saline water covers the entire inland sea. In April there is no distinct circulation pattern, except for Bungo Channel. The outward flow of 0.03–0.04 m s^{-1} is clearly seen in Bungo Channel, forming an inverse estuarine circulation along with the surface current (Fig. 9(a)).

In summer, the bottom current becomes intensive

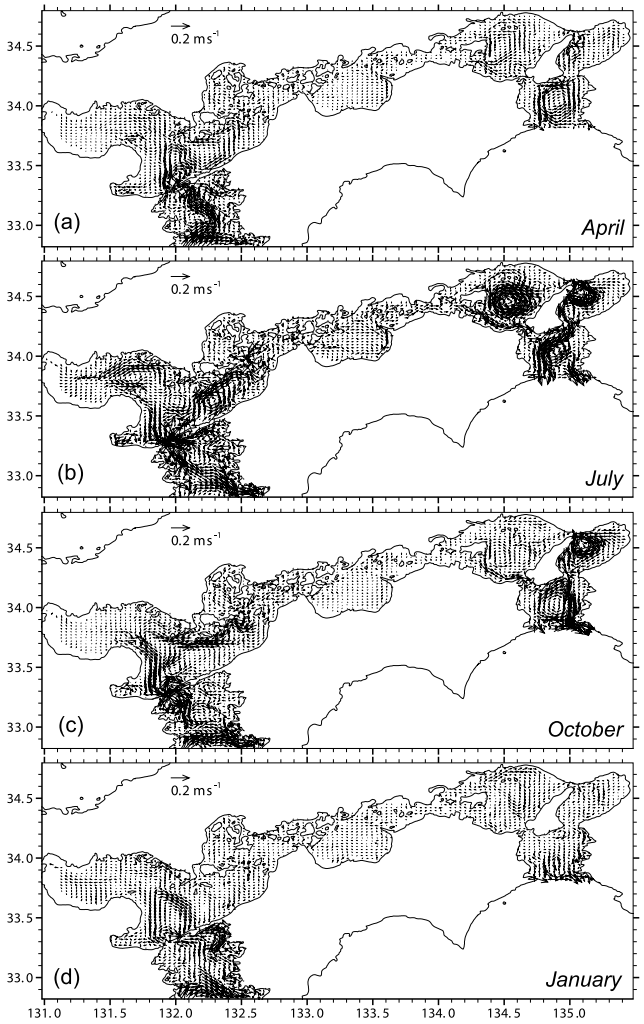

Fig. 9. Monthly mean surface residual current distributions at 10 m depth in (a) April, (b) July, (c) October, and (d) January, after subtracting tide-induced residual current shown in Fig. 8.

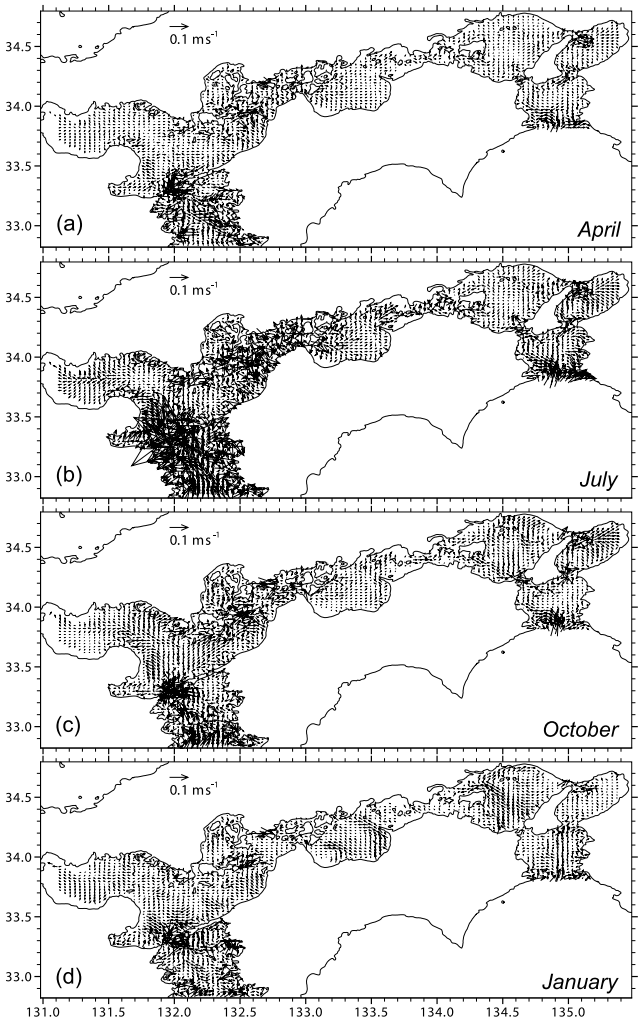

Fig. 10. As Fig. 9, but for near-bottom current fields.

especially in the western part of SIS; an inflow of about 0.05 m s^{-1} exists in Bungo Channel, and a non-organized but inward flow pattern is shown in Aki-Nada (Fig. 10(b)). The inward flow pattern extends to the Bisan Strait. Although the bottom current is weak in the eastern SIS, it is also directed to the inner sea. It appears that the inflows from the western and eastern SIS converge at Bisan Strait. In addition, the bottom current is weak in the regions where the cyclonic circulations exist in the surface layer; in particular, divergence is found in Suo- and Iyo-Nada.

Associated with the disappearance of cyclonic eddies, the divergence in bottom layer can no longer be discerned (Fig. 10(c)). Simultaneously, the flow toward the inside SIS becomes intense. It is likely that a two-layer opposite flow (i.e., estuarine circulation) becomes strong in autumn, especially in Suo- and Iyo-Nada. Moreover, the alongshore current in the Harima-Nada to the Bisan Strait becomes stronger, and a typical up-estuarine flow is found in the eastern Osaka Bay.

The near-bottom flow to the inside SIS is no longer dominant in winter (Fig. 10(d)). On the whole, the bottom current opposite the northwesterly wind develops in the SIS. In the Hiuchi- and Harima-Nada, the upwind currents are stronger in the deeper region than the shallow water. Moreover, an eddy-like flow pattern is displayed in the northern Harima-Nada. These winter circulation patterns are examined more detail in Subsection 4.4.

4.3 Cyclonic circulation: summer feature

Summer current fields described in the previous section demonstrate that the cyclonic eddies are dominant in several Nadas where tidal mixing is relatively weak. Al-

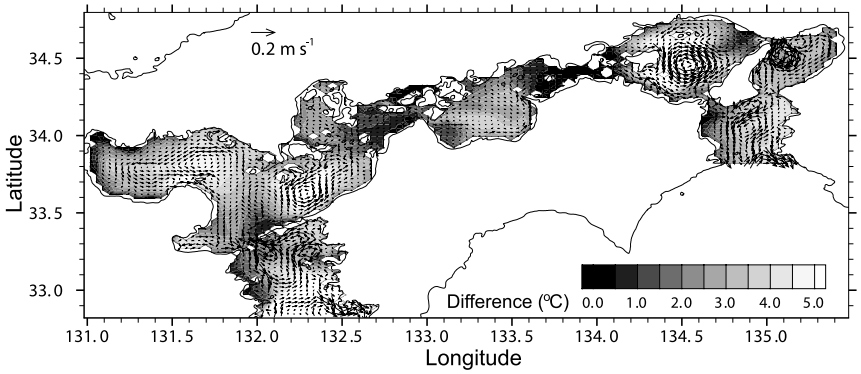

Fig. 11. Temperature difference between surface and bottom layers in July. Vectors indicate vertically averaged residual current after subtracting tide-induced residual current.

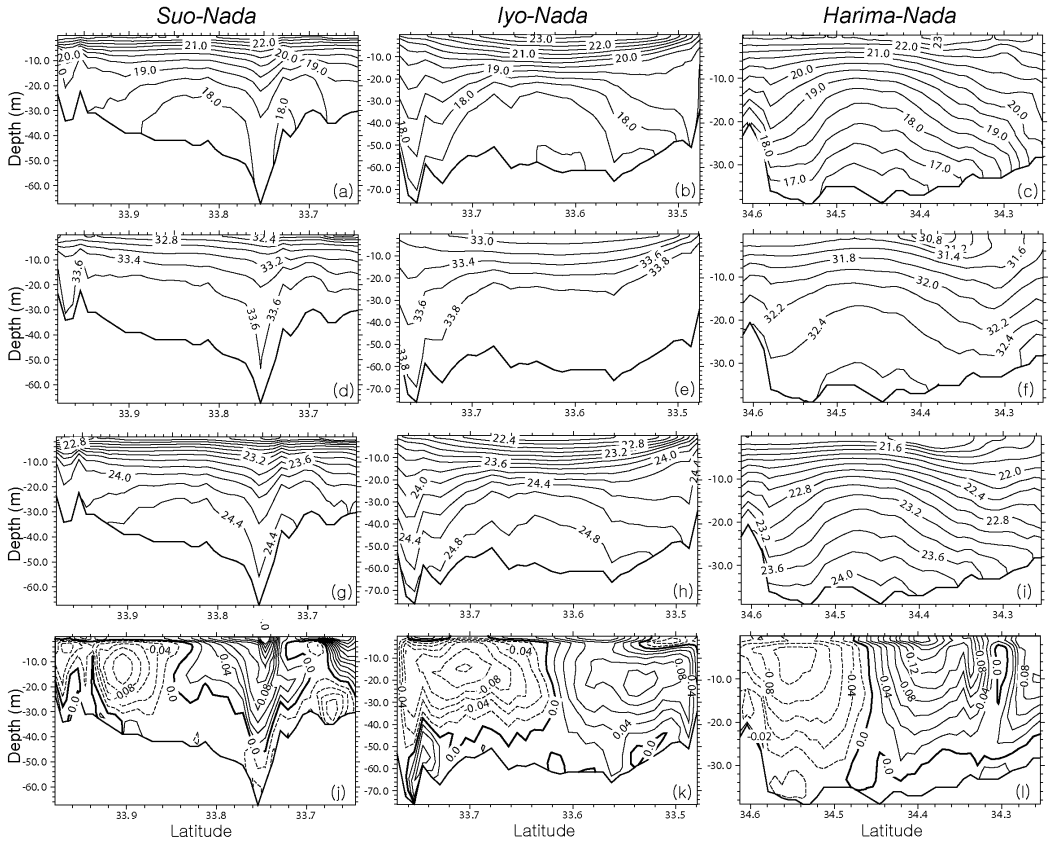

Fig. 12. Monthly mean cross-sectional distributions of (a)–(c) temperature (°C); (d)–(f) salinity (psu); (g)–(i) density, σ_t; (j)–(l) normal velocity (m s^{-1}) for the Suo- (left panels), Iyo- (middle panels), and Harima-Nada (right panels) in July. See Fig. 2 for location of the sections.

though the current fields in Fig. 9(b), in which tidal residual flow is subtracted, also include a wind-driven component and nonlinear interaction of the residual flow, it is mostly driven by the density gradient because of weak summer winds. Figure 11 indicates the temperature difference between the surface and bottom layers as well as vertically averaged current fields after removing tide residual flow. Since outward flow in the surface layer is canceled by inward flow in the bottom layer, the cyclonic eddies become salient. Due to strong tidal mixing, tem-

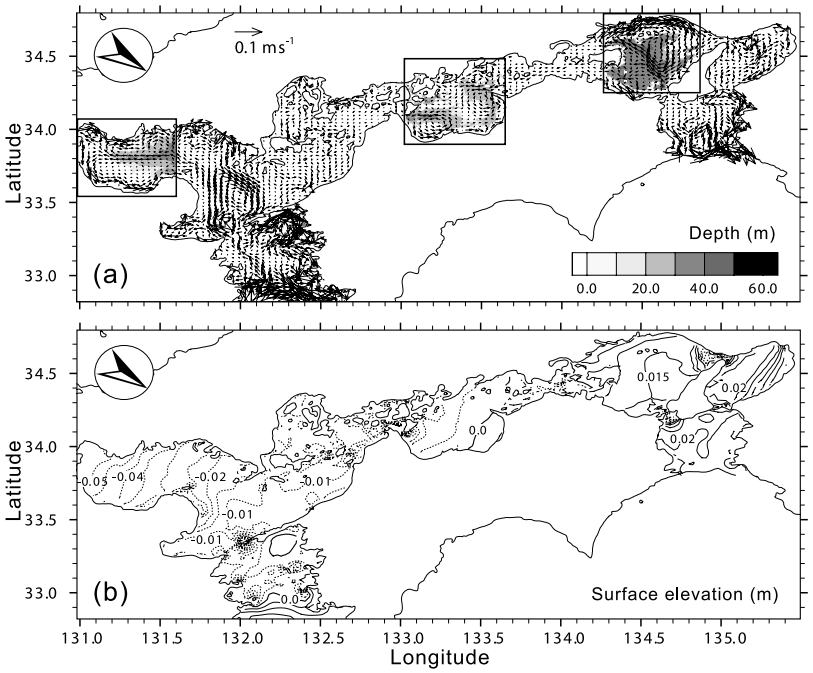

Fig. 13. Monthly mean distributions of (a) vertically averaged current field and (b) surface elevation in January. Grids deeper than the average water depth in each Nada (surrounded by three boxes) are shaded. Spatially averaged wind direction is given in upper-left corner of each panel.

perature difference is negligible near the straits. By contrast, thermal stratification is strong in the Nadas, where the cyclonic eddies are clearly overlapped by the large temperature difference (see the light colored region; $\Delta t >$ 4.0°C). On the other hand, the salinity difference does not indicate a distinct relationship with the cyclonic circulation (not shown). Since the temperature structure is mostly responsible for the density structure in those Nadas, that in turn induces the cyclonic circulation.

Figure 12 presents vertical distributions of temperature, salinity, density and normal velocity at sections in the Suo-, Iyo- and Harima-Nada in July where cyclonic eddies are established (see marked solid line in Fig. 2 for sections). An increase of solar heating and river run-off induce high temperature and low salinity water in the surface layer during summer. Although its scale is different, the warm pool is also discernible in the surface layer, especially in Iyo-Nada. The most remarkable structure is the cold dome of about 16.0–18.0°C beneath the thermocline in the middle of each Nada (Figs. 12(a)–(c)). Although a similar structure is shown in the salinity distribution of Harima-Nada, it is considered that the temperature (i.e., cold dome) is most responsible for the symmetric density structure. Associated with these cold domes are the cyclonic flows that are in geostrophic balance with the density fields through the thermal wind relation (Figs. 12(j)–(l)). The cyclonic flow reveals a robust horizontal structure. In addition, high velocities of about 0.1 m s^{-1} exist in the subsurface layer; this feature is particularly distinct in Iyo-Nada, because of the interference of anticyclonic flow in the surface layer due to the warm pool (Davis and Xing, 2006).

Based on ship-mounted ADCP and CTD observations, Guo *et al*. (2006) revealed an eddy structure in the velocity field in Iyo-Nada during late July, 2005. Note that their observation section is located near the marked line in Fig. 2. The cyclonic subtidal current has a magnitude of 0.1–0.2 m s^{-1}; the outflow reaches around 0.2 m s^{-1}, while the inflow is less than 0.1 m s^{-1} in the subsurface layer. Although the model could not directly compare with the above field observation, it is considered that the model results are comparable to observations made in the Iyo-Nada during summer.

As inferred from horizontal current fields in Figs. 9 and 10, an estuarine circulation exists in the SIS during summer and autumn. We can confirm the flow structure in the velocity section of northern Iyo-Nada (>33.7°N) and southern Suo-Nada (i.e., offshore Kunisaki Peninsula, <33.7°N). It is expected that the sharp gradient of low salinity water induces those circulations there, implying that the increased freshwater input during summer has an influence on the circulation in the SIS. The roles of freshwater discharge in the summer and autumn circulation are discussed in Section 5.

4.4 Wind-driven circulation: winter feature

As shown in the vertical distributions of temperature and salinity (Fig. 7), the water in winter is vertically well mixed, except for Osaka Bay. On the other hand, the strong northwesterly wind stress is predominant in the whole inland sea. To examine wind effects on the circulation, we begin with the vertically averaged current fields in January (Fig. 13(a)). The computed current field reveals that it is downwind in the shallow coastal region, while a upwind current concentrates at deep parts of the Nadas (see shaded region), forming basin-scale eddies: a double-gyre in the Suo-Nada, and two cyclonic eddies in Hiuchi-Nada and an anticyclonic eddy in Harima-Nada. Besides those eddies, a southward coastal current is found in the eastern part of Bungo and Kii Channels, while a strong anticyclonic current is developed in western Iyo-Nada, supplying warm and salt water into Suo-Nada. Figure 13(b) shows the surface elevation during the same periods. The distribution of sea level shows that the sea level is high at the eastern part in each Nada and low at the straits, as examined in Fujiwara and Higo (1986). In general, sea level slope confronts the northwesterly winds throughout the whole SIS, suggesting that the geostrophic component only could not explain the flow patterns described above.

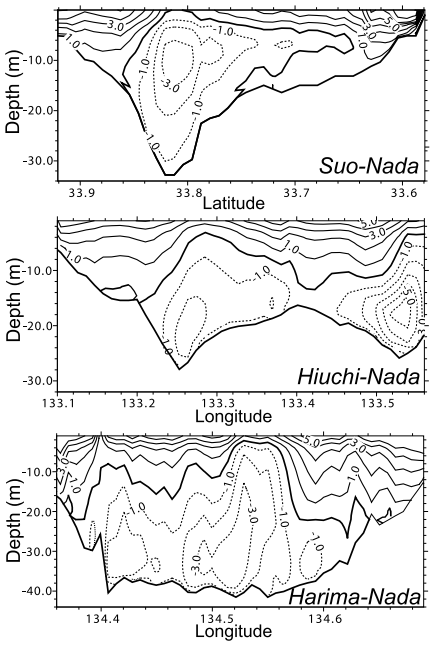

Fig. 14. Monthly mean cross-sectional distributions of normal velocity (m s^{-1}) for the Suo- (upper panel), Hiuchi- (middle panel), and Harima-Nada (lower panel). Note that positive (negative) values indicate downwind (upwind) current. See marked dotted lines in Fig. 2 for position of sections. Contour interval is 0.01 m s^{-1}.

Here we describe the vertical distributions of above eddies, adopting sections marked in Fig. 2 (see thick dotted lines). Note that negative (positive) values represent upwind (downwind) in normal velocity component. From the modeled results, it can be seen that the wind drives downwind circulation throughout the water column over the shallow water (Fig. 14(a)). The maximum velocity, over 0.05 m s^{-1}, exists at the surface layer, and the velocity decreases with increasing bottom friction. On the other hand, the upwind current is predominant in the deep region, and the current core is found at the mid-layer in Suo-Nada and the deeper layer in Hiuchi- and Harima-Nada. When considering the distribution of surface elevation, it is expected that the pressure gradient forcing due to the sea level slope induces the upwind current in the deep region (deeper than average water depth), as described by Csanady (1982).

To elucidate the effect of wind forcing, we performed an additional experiment without wind forcing. Figure 15 shows the vertically averaged current fields in the without-wind case. There is no distinct circulation pattern in the results of the without-wind case, and the circulation in shallow water, such as eddies in Suo-, Hiuchi-, and Hriama-Nada, is no longer discerned. By contrast, an

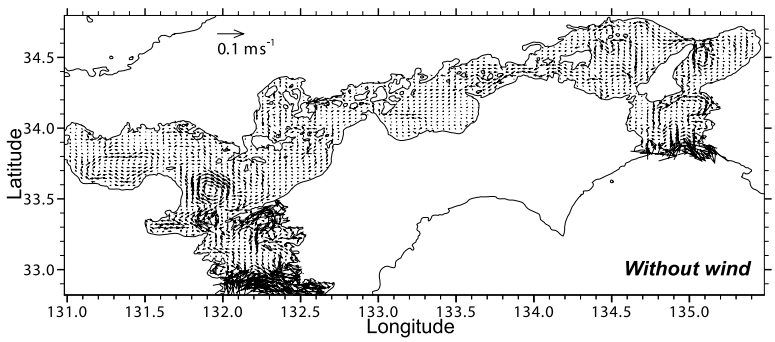

Fig. 15. Vertically averaged current distribution in January, obtained from without-wind experiment.

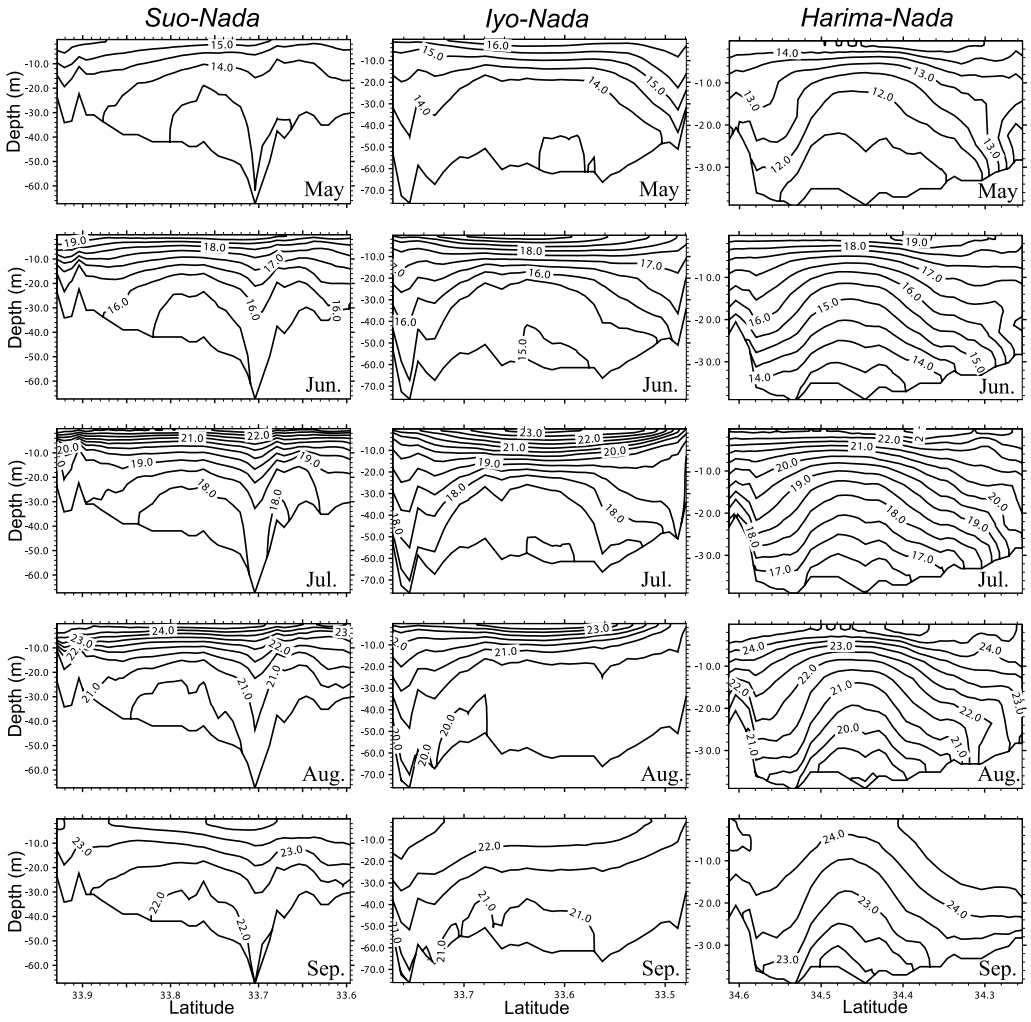

Fig. 16. Monthly variations of the temperature at sections across cyclonic eddies in the Suo- (left panels), Iyo- (middle panels), and Harima-Nada (right panels) from May to September. Contour interval is 1.0°C.

outward flow pattern along the deep region in Suo-Nada appears due to the gravitational effect of dense water in a shallow region. The without-wind experiment evidently indicates that the eddies shown in shallow Nada are mostly wind-driven. In addition, the winter wind reinforces the anticyclonic circulation in the western Iyo-Nada.

5. Conclusions and Discussion

A high-resolution, three dimensional numerical ocean model based on the POM has been applied to the SIS to simulate the seasonal variation of general circulation. Annually varying forcings, such as surface fluxes, river discharge and lateral flux are imposed on the model sea, as well as tidal forcing. Since this is the first time that the three dimensional model with realistic conditions has been applied to the entire SIS, the general circulation features obtained by the model are presented and compared with observation. The model reproduces well the observations of long-term mean surface current and hydrographic features, and the simulated water circulation reveals remarkable seasonal variability. The seasonal variation of current field is summarized below.

In early spring there are no remarkable currents in the Nadas, but inverse estuarine circulation and a cyclonic eddy are established in Bungo and Kii Channels, respectively. As stratification becomes strong during summer, cyclonic eddies associated with a cold dome appear in several Nadas, such as Suo-, Iyo-, and Harima-Nada. Moreover, an outward flow toward Bungo and Kii Channels exists in the surface layer, while there is an inward flow near the bottom layer. The cyclonic eddies disappear in autumn, while the two-layer opposite circulation system remains. In winter, the surface current exhibits a relatively weak circulation. During this period the anti-

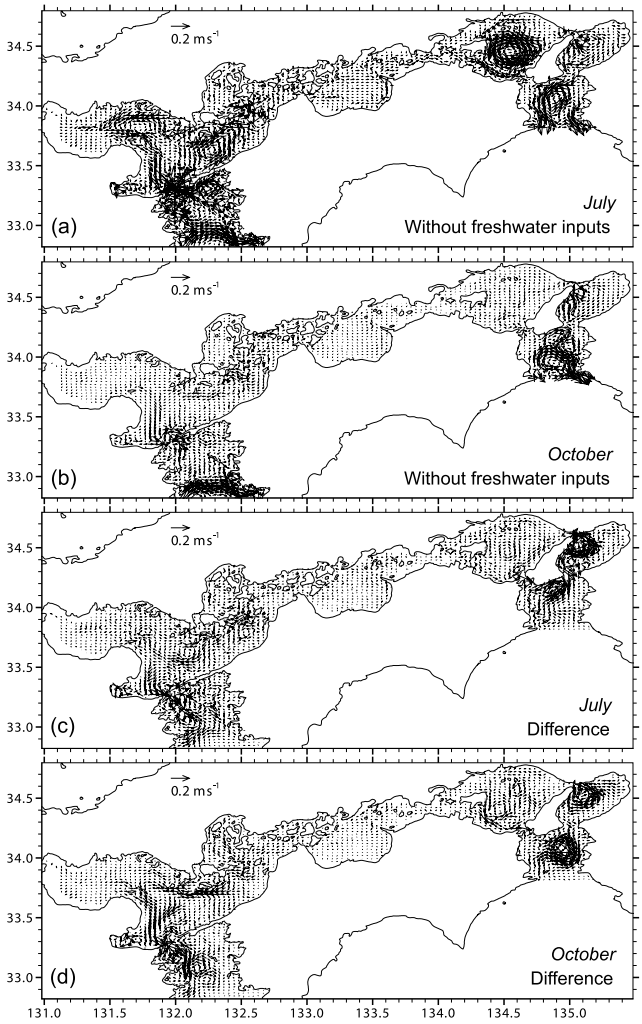

Fig. 17. Simulated surface current distributions for the case of without freshwater input, in (a) July and (b) October. Also given are differences between cases with and without freshwater input in (c) July and (d) October.

cyclonic circulation in the western Iyo-Nada is developed, and the current below the surface layer generally shows an oppositely directed flow to the intense northwesterly wind stress, especially over the deep water of Suo-, Hiuchi-, and Harima-Nada.

One of the most important implications of our model results relates to the presence of a cold dome, which is substantial in the summer circulation. The sharp pressure gradient due to the cold dome is the main forcing that generates cyclonic eddies in the Nadas. To examine the temporal variation of the cold dome, here we illustrate the vertical temperature distributions from May to September at each Nada (Fig. 16). The model results indicate that the cold dome generally forms in May and weakens from August. With the extinction of the cold dome, cyclonic eddies also disappear in our model. The rate of temperature change in the cold dome is roughly 2.0–2.6 °C month^{-1} during the warming season (May–August), which is similar to that in the surface layer (2.5–3.2 °C month^{-1}). When considering strong summer stratification, this implies that the horizontal advection/mixing might play an important role in supplying heat from the surrounding well-mixed region to the cold dome (e.g., Takeoka, 1985, 2002).

In addition to the thermal structure, freshwater discharge during summer has also a great effect on the density distribution in the SIS (Takeoka, 1985). To elucidate the effect of freshwater input, a simple experiment without freshwater input was carried out after the model had achieved a stable state. The noticeable differences in flow fields with and without freshwater input are mostly revealed in the summer and autumn periods. Figure 17 shows surface current without freshwater input in July and October (Figs. 17(a) and (b)), and the difference between cases with and without freshwater input in the same months (Figs. 17(c) and (d)). The current field without freshwater influx in July is similar to the major summer circulation in Fig. 9(b), showing cyclonic eddies in the Nadas. However, a relatively large difference is found in the outward flow (Fig. 17(c)): outward surface currents from Iyo Nada (Osaka Bay) to Bungo Channel (Kii Channel).

The effect of freshwater input is more apparent in October. It can be seen that there is no remarkable flow pattern in the SIS, except in both channels (Fig. 17(b)). As in summer, the outward velocity anomaly is pronounced in the difference plot (Fig. 17(d)), showing a similar pattern to the surface current field in autumn (see Fig. 9(c)). This is also the same for the inward flow near the bottom layer (not shown). It is therefore clear that the freshwater influx underlies the maintenance of the strong estuarine circulation in the transition periods, which is represented in the present model study.

The validated model could be useful in understanding a basic winter circulation feature in the SIS, in which observations of flow velocity are deficient during the winter season. The computed winter circulation demonstrates that the intense winter wind has a significant effect on the circulation in the SIS. Since the water is well mixed throughout the water column during winter, the intense wind stress easily acts on the deeper water. The downwind current is thus dominant over the shallow water of each Nada, implying that acceleration due to wind stress is stronger than the pressure gradient. By contrast, in the region where the depth is deeper than average, the pressure gradient induces an upwind current. As a consequence, the vertically integrated flow pattern represents an eddy structure in several Nadas: a "double-gyre pattern" in the Suo-Nada, two anticyclonic eddies in Hiuchi-

Nada, and anticyclonic circulation in Harima-Nada.

The present study shows that the cold dome is an important water structure that determines the summer circulation in several Nadas. Based on the field observations in 2004 and 2005, Guo *et al*. (2006) reported a significant inter-annual variability of the cold dome in the Iyo-Nada and suggested the possibility of a competition between the cyclonic eddy and estuarine circulation in Iyo-Nada, which is located on the pathway of a basin-scale estuarine circulation in the SIS. For a full understanding of such field observations, it is necessary to clarify the factors controlling the formation of cold domes in the SIS. The fact that the cold dome and the surface layer above have a similarly increasing rate of temperature indicates the importance of horizontal advection/mixing process between the stratified water in the Nadas and ambient homogeneous water in the straits. Our next study will examine the different role of horizontal and vertical processes in heat and salt transports in the SIS, a fundamental issue related to the formation of the cold dome.

Acknowledgements

The authors express their sincere thanks to two anonymous reviewers for their useful comments. P.-H. Chang is grateful for the financial support from the Japan Society for the Promotion of Science (JSPS), Postdoctoral Fellowship for Foreign Researchers. The study was also supported by a Grant-in-Aid for the Global COE Program from the Ministry of Education, Culture, Sports, Science and Technology, Japan (MEXT), and the Japan Society for the Promotion of Science (JSPS).

References

Awaji, T., N. Imasato and H. Kunishi (1980): Tidal exchange through a strait: A Numerical experiments using a simple model basin. *J. Phys. Oceanogr.*, **10**, 1499–1508.

Balotro, R. S., A. Isobe, M. Shimiz, A. Kaneda, T. Takeuchi and H. Takeoka (2002): Circulation and material transport in Suo-Nada during spring and summer. *J. Oceanogr.*, **58**, 759–773.

Blumberg, A. F. and G. L. Mellor (1987): A description of a three dimensional coastal ocean circulation model. p. 1–16. In *Three-Dimensional Coastal Ocean Models, Coastal Estuarine Stud.*, Vol. 4, ed. by N. Heaps, AGU, Washington, D.C.

Csanady, G. T. (1982): *Circulation in the Coastal Ocean*. D. Reidel, 279 pp.

Davis, A. M. and J. Xing (2006): Effects of topography and mixing parameterization upon the circulation in cold water domes. *J. Geophys. Res.*, **111**, C03018, doi:10.1029/2005JC003066.

Flather, R. A. (1976): A tidal model of the northwest European continental shelf. *Mem. Soc. Roy. Sci. Liege*, **10**, 141–164.

Fujiwara, M., K. Ohashi and T. Fujiwara (1997): Simulation of residual flow in Kii Channel in August by using a diagnostic numerical model. *Proceedings of Coastal Engineering*, **44**, 411–415 (in Japanese).

Fujiwara, T. and T. Higo (1986): Wind effects on the through flow and material transport in the Seto Inland Sea. *Bull. Coast. Oceanogr.*, **23**, 109–119 (in Japanes).

Fujiwara, T., T. Higo and Y. Takasugi (1989): On the residual circulations, tidal flows, and eddies in Osaka Bay. *Proc. 36th Conf. on Coastal Engineering*, JSCE, 209–213 (in Japanese).

Fujiwara, T., H. Nakata and K. Nakatsuji (1994): Tidal-jet and vortex-pair driving of the residual circulation in a tidal estuary. *Cont. Shelf Res.*, **14**, 1025–1038.

Guo, X. (2005): Toward prediction of marine environment in the Seto Inland Sea, Japan. *Monthly Kaiyo*, **37**, 289–293 (in Japanese).

Guo, X., H. Hukuda, Y. Miyazawa and T. Yamagata (2003): A triply nested ocean model for simulating the Kuroshio—Roles of horizontal resolution on JEBAR. *J. Phys. Oceanogr.*, **33**, 146–169.

Guo, X., A. Futamura and H. Takeoka (2004): Residual currents in a semi-enclosed bay of the Seto Inland Sea, Japan. *J. Goephys. Res.*, **109**, C12008, doi:10.1029/2003JC002203.

Guo, X., M. Haramoto, P.-H. Chang, A. Futamura and H. Takeoka (2006): Competition of a local cyclonic eddy and an estuarine circulation in the Iyo-nada, Seto Inland Sea, Japan. *Proceedings of the 13th International Biennial Conference on Physics of Estuaries and Coastal Seas*, Astoria, U.S.A.

Hill, A. E. (1994): Observations of a cyclonic gyre in the western Irish Sea. *Cont. Shelf Res.*, **14**, 479–490.

Hill, A. E. (1996): Spin-down and the dynamics of dense pool gyres in shallow seas. *J. Mar. Res.*, **54**, 1–17.

Hirose, N., H.-C. Lee and J.-H. Yoon (1999): Surface heat flux in the East China Sea and the Yellow Sea. *J. Phys. Oceanogr.*, **29**, 401–417.

Horsburgh, K. J. and A. E. Hill (2003): A three-dimensional model of density-driven circulation in the Irish Sea. *J. Phys. Oceanogr.*, **33**, 343–365.

Imasato, N., T. Awaji and H. Kunishi (1980): Tidal exchange through Naruto, Akashi and Kitan Straits. *J. Oceanogr. Soc. Japan*, **36**, 151–162.

Kamizono, M., M. Yoshida, M. Ishida and T. Miita (1991): Surface current investigation in Suo-Nada using drift bottles. *Bull. Coast. Oceanogr.*, **29**, 97–103 (in Japanese with English abstract).

Kasai, A., T. Yamada and H. Takeda (2007): Flow structure and hypoxia in Hiuchi-Nada, Seto Inland Sea, Japan. *Estuar., Coast. Shelf Sci.*, **71**, 210–217.

Kim, Y. S. and R. Kimura (1995): Error evaluation of the bulk aerodynamic method for estimating heat flux over the sea. *J. Korean Meteor. Soc.*, **31**, 399–413.

Kobayashi, S., J. H. Simpson, T. Fujiwara and K. J. Horsburgh (2006): Tidal stirring and its impact on water column stability and property distributions in a semi-enclosed shelf sea (Seto Inland Sea, Japan). *Cont. Shelf Res.*, **26**, 1295–1306.

Large, W. G. and S. Pond (1981): Open ocean momentum flux measurement in moderate to strong winds. *J. Phys. Oceanogr.*, **11**, 323–336.

Matsumoto, K., T. Takanezawa and M. Ooe (2000): Ocean tide models developed by assimilating TOPEX/POSEIDON altimeter data in to hydrodynamical model: a global model and a regional model around Japan. *J. Oceanogr.*, **56**, 567–581.

Mellor, G. L. and T. Yamada (1982): Development of a turbulence closure model for geophysical fluid problems. *Rev. Geophys.*, **20**, 851–875.

Murakami, M., Y. Oonishi, A. Harashima and H. Kunishi (1978): A numerical simulation on the distribution of water temperature and salinity in the Seto Inland Sea. *Bull. Coast. Oceanogr.*, **15**, 130–137.

Murakami, M., Y. Oonishi and H. Kunishi (1985): A numerical simulation of the distribution of water temperature and salinity in the Seto Inland Sea. *J. Oceanogr. Soc. Japan*, **41**, 213–244.

Ochi, T. and H. Takeoka (1986): The anoxic water mass in Hiuchi Nada. Part I. Distribution of the anoxic water mass. *J. Oceanogr. Soc. Japan*, **42**, 1–11.

Oonishi, Y. (1977): A numerical study on the tidal residual flow. *J. Oceanogr. Soc. Japan*, **33**, 207–218.

Oonishi, Y. (1979): A numerical experiment on the constant flow in Osaka Bay. *Proc. 26th Conf. on Coastal Engineering*, JSCE, 514–518 (in Japanese).

Smagorinsky, J. S. (1963): General circulation experiments with the primitive equations. I. The basic experiment. *Mon. Wea. Rev.*, **91**, 99–164.

Takeoka, H. (1985): Density stratification in the Seto Inland Sea. *Umi to Sora*, **60**, 145–152 (in Japanese).

Takeoka, H. (2002): Progress in Seto Inland Sea research. *J. Oceanogr.*, **58**, 93–107.

Tawara, S. (1986): Studies on the characteristics of oceanographic condition in relation to fishing condition in the shallow coastal waters. *J. Shimonoseki Univ. Fisheries*, **34**(1), 1–103.

Xing, J. and A. M. Davis (2001): A three-dimensional baroclinic model of the Irish Sea: Formation of the thermal fronts and associated circulation. *J. Phys. Oceanogr.*, **31**, 94–114.

Yanagi, T. and H. Higuchi (1979): Constant flows in the Seto Inland Sea. *Bull. Coast. Oceanogr.*, **16**, 123–127.

Yanagi, T. and S. Igawa (1992): Diagnostic model in the coastal sea—an application to Suo-Nada and Iyo-Nada. *Bull. Coast. Oceanogr.* **30**, 108–115 (in Japanese with English abstract).

Yanagi, T. and S. Okada (1993): Tidal fronts in the Seto Inland Sea. *Mem. Fac. Eng. Ehime Univ.*, **12**(4), 337–343.